Iron−Rhodium and Iron−Iridium Mixed-Metal Nitrido−Carbonyl Clusters. Synthesis, Characterization, Redox Properties, and Solid-State Structure of the Octahedral Clusters $[Fe_5RhN(CO)_{15}]^{2-}$, $[Fe_5IrN(CO)_{15}]^{2-}$, and $[Fe_4Rh_2N(CO)_{15}]^{-}$. Infrared and Nuclear Magnetic Resonance Spectroscopic Studies on the Interstitial Nitride

Roberto Della Pergola,*,† Arnaldo Cinquantini,‡ Eliano Diana,§ Luigi Garlaschelli,† Franco Laschi,‡ Paola Luzzini,† Mario Manassero,*,|| Andrea Repossi,† Mirella Sansoni,|| Pier Luigi Stanghellini,*,§ and Piero Zanello*,‡

Dipartimento di Chimica Inorganica, Metallorganica ed Analitica and Centro del CNR, Università di Milano, via G. Venezian 21, 20133 Milano, Italy, Dipartimento di Chimica Strutturale e Stereochimica Inorganica and Centro del CNR, Università di Milano, via G. Venezian 21, 20133 Milano, Italy, Dipartimento di Chimica I.F.M., Università di Torino, via P. Giuria 7, 10125 Torino, Italy, and Dipartimento di Chimica dell' Università, Pian dei Mantellini 44, 53100 Siena, Italy

Received December 4, 1996[⊗]

The cluster $[Fe_5RhN(CO)_{15}]^{2-}$ was synthesized in 40% yield from $[Fe_4N(CO)_{12}]^{-}$ and $[Rh(CO)_4]^{-}$ in refluxing tetrahydrofuran, whereas the analogous anion $[Fe_5IrN(CO)_{15}]^{2-}$ was prepared in CH_3CN at room temperature from $[Fe_6N(CO)_{15}]^{3-}$ and $[Ir(C_8H_{14})_2Cl]_2$; the yields are higher than 60%. The monoanion $[Fe_4Rh_2N(CO)_{15}]^{-}$ was obtained in 70% yield from $[Fe_5RhN(CO)_{15}]^{2-}$ and hydrated $RhCl_3$. The solid-state structures of the three anions were determined on their $[PPh_4]^{+}$ salts: the six metal atoms are arranged in octahedral cages and are coordinated to 3 edge-bridging and 12 terminal carbonyl ligands and to a μ_6-N ligand. The Rh and Ir atoms have less terminal COs than Fe, in order to equalize the excess electrons at the d^9 metal centers. The two rhodium atoms in $[Fe_4Rh_2N(CO)_{15}]^{-}$ are directly bound. The ^{15}N NMR spectra of the three compounds have been recorded; the signals of the nitride ligands were found at $\delta = 514$ ppm for the dianions and 470 ppm for $[Fe_4Rh_2N(CO)_{15}]^{-}$; any group 9 atom shifts the resonance of nitrogen to higher fields. The coupling constants $J(^{15}N-^{103}Rh)$ are 8−9 Hz. The vibrational patterns of the metal cores have been interpreted on the basis of an idealized M_6 octahedral arrangement, subsequently modified by the perturbations given by different atomic masses and M−M stretching force constants. The motions of the nitrogen are related to the idealized symmetry of the cage; the M−N force constant values depend on the type of metal and on the charge of the anion. The dianions $[Fe_5MN(CO)_{15}]^{2-}$ can be electrochemically oxidized at −20 °C to their short-lived monoanions, which can be characterized by EPR spectroscopy. In contrast, the cluster $[Fe_4Rh_2N(CO)_{15}]^{-}$ undergoes a single-step 2-electron reduction to the partially stable trianion $[Fe_4Rh_2N(CO)_{15}]^{3-}$, which was also characterized by EPR spectroscopy. The Fe−Rh nitride clusters are active catalysts for the hydroformylation of 1-pentene, but display low selectivity (35−65%) in *n*-hexanal and are demolished under catalytic conditions.

In 1981, Muetterties described the synthesis of several mixed-metal carbide clusters, obtained by polyhedral expansion of $[Fe_4C(CO)_{12}]^{2-}$ or $[Fe_5C(CO)_{14}]^{2-}$.[1] The square-based pyramidal or octahedral metal cages of the heteronuclear clusters were assessed by solving the solid-state structures of $[Fe_4RhC(CO)_{14}]^{-}$ and $[Fe_5MoC(CO)_{17}]^{2-}$.[2] Almost at the same time, the same author described the synthesis of two iron nitride clusters, $[Fe_4N(CO)_{12}]^{-}$ and $[Fe_5N(CO)_{14}]^{-}$, and the solid-state structure of the corresponding hydrides $[HFe_4N(CO)_{12}]$ and $[HFe_5N(CO)_{14}]$.[3] Much more recently, Fehlner *et al.* reported the preparation, characterization, and skeletal transformation of the *cis* and *trans* isomers of $[Fe_4Rh_2B(CO)_{16}]^{-}$.[4,5] In order to expand the series of heteronuclear clusters containing B, C, or N as interstitial ligands, we considered attempting to synthesize mixed metal Fe−M−N clusters worthwhile; the first efforts focused on the Fe−Rh[6] and Fe−Ir[7] systems, since we have experience in these fields. In this paper the first results in this area are described, namely the characterization, electrochemical properties, and structures of $[Fe_5RhN(CO)_{15}]^{2-}$ (**1**), $[Fe_5IrN(CO)_{15}]^{2-}$ (**2**), and $[Fe_4Rh_2N(CO)_{15}]^{-}$ (**3**), together with the

† Dipartimento di Chimica Inorganica, Metallorganica ed Analitica and Centro del CNR.

‡ Dipartimento di Chimica dell' Università.

§ Dipartimento di Chimica I.F.M.

|| Dipartimento di Chimica Strutturale e Stereochimica Inorganica and Centro del CNR.

⊗ Abstract published in *Advance ACS Abstracts,* July 15, 1997.

(1) Tachikawa, M.; Geerts, R. L.; Muetterties, E. L. *J. Organomet. Chem.* **1981**, *213*, 11.

(2) Tachikawa, M.; Sievert, A. C.;Thompson, M. R.; Day, C. S.; Day, V. W.; Muetterties, E. L. *J. Am. Chem. Soc.* **1980**, *102*, 1725.

(3) Tachikawa, M.; Stein, J.; Muetterties, E. L.; Teller, R. G.; Beno, M. A.; Gebert, E.; Williams, J. M. *J. Am. Chem. Soc.* **1980**, *102*, 6649.

(4) (a) Khattar, R.; Puga, J.; Fehlner, T. P.; Rheingold, A. L. *J. Am. Chem. Soc.* **1989**, *111*, 1879. (b) Bandyopadhyay, A. K.; Khattar, R.; Fehlner, T. P. *Inorg. Chem.* **1989**, *28*, 4436.

(5) Bandyopadhyay, A. K.; Khattar, R.; Puga, J.; Fehlner, T. P.; Rheingold, A. L. *Inorg. Chem.* **1992**, *31*, 465.

(6) (a) Ceriotti, A.; Longoni, G.; Sansoni, M.; Della Pergola, R.; Heaton, B. T.; Smith, D. O. *J. Chem. Soc., Chem. Commun.* **1982**, 886. (b) Ceriotti, A.; Longoni, G.; Della Pergola, R.; Heaton, B. T.; Smith, D. O. *J. Chem. Soc., Dalton Trans.* **1983**, 1433. (c) Della Pergola, R.; Fracchia, L.; Garlaschelli, L.; Manassero, M.; Sansoni, M. *J. Chem. Soc., Dalton Trans.* **1995**, 2763.

(7) (a) Della Pergola, R.; Ceriotti, A.; Garlaschelli, L.; Demartin, F.; Manassero, M.; Masciocchi, N. *Inorg. Chem.* **1993**, *32*, 3349. (b) Ceriotti, A.; Della Pergola, R.; Garlaschelli, L.; Laschi, F.; Manassero, M.; Masciocchi, N.; Sansoni, M.; Zanello, P. *Inorg. Chem.* **1991**, *30*, 3349.

S0020-1669(96)01451-6 CCC: $14.00

spectroscopic behavior of the interstitial nitride ligand and the vibrational deformations of the metal cages (^{15}N NMR, solid-state IR and Raman spectroscopies).

In contrast to what might be expected,[1] the anionic $[Fe_4N(CO)_{12}]^-$ does not react with soft electrophiles and the polyhedral expansion could only be obtained with the strongest nucleophiles, such as $[Rh(CO)_4]^-$ or $[Fe_2(CO)_8]^{2-}$. The synthesis of **2** or **3** was achieved by metal substitution on preformed octahedral frames; up to now, no tetra- or pentanuclear mixed-metal nitride clusters have been isolated.

Clusters **1** and **3** have also been used for the hydroformylation of 1-pentene, as a measure of their stability relative to the corresponding Fe−Rh carbides.[8]

Results

Synthesis. Synthesis of $[Fe_5RhN(CO)_{15}]^{2-}$ (1). The dianion **1** was obtained by reacting equimolar amounts of $[Fe_4N(CO)_{12}]^-$ and $[Rh(CO)_4]^-$ in refluxing tetrahydrofuran (THF). After about 4 h the reaction is complete. Although the yields are in the range 35−40%, the reaction is fairly selective and the only product present in the solution is $[Fe_5RhN(CO)_{15}]^{2-}$. A black uncharacterized material, insoluble in most common organic solvents, is the only byproduct. Therefore, the mixed-metal cluster can be easily recovered by filtration and crystallization from THF/2-propanol. The rather low yields could be anticipated, considering that the Fe:Rh:N:negative charge ratios in the reagents is not matching that of the final product. Therefore, a considerable fraction of $[Fe_4N(CO)_{12}]^-$ must be decomposed to generate iron carbonyl fragments.

The formation of **1** from $[Fe_4N(CO)_{12}]^-$ and an anionic carbonyl complex is similar to the synthesis of $[Fe_6N(CO)_{15}]^{3-}$ (**4**), which was also obtained by polyhedral expansion by reacting $[Fe_4N(CO)_{12}]^-$ and $[Fe_2(CO)_8]^{2-}$.[9] These condensations are also in keeping with the findings that the electrochemically generated dianion $[Fe_4N(CO)_{12}]^{2-}$ has limited stability, whereas the $[Fe_4N(CO)_{12}]^-$ is immediately decomposed under oxidative conditions.[10]

Synthesis of $[Fe_5IrN(CO)_{15}]^{2-}$ (2). The reaction between $[Fe_4N(CO)_{12}]^-$ and $[Ir(CO)_4]^-$ at the temperature of refluxing THF does not proceed. In order to detect the formation of new products, the reaction had to be carried in refluxing diglyme (2-methoxyethyl ether, boiling point 162 °C).[3] Even better, the condensation between the reagents could be promoted by additions of Na-ketyl in THF solution. The strong reductant was used since it has been observed that carbonyl dissociation from $[Fe_4N(CO)_{12}]^-$ is catalyzed by reductants;[10] this promotion, however, cannot induce well behaving reactions, since the average oxidation state of the metals (−0.33) in the final product is higher than that in the starting material (−0.4). Both reactions yielded very tiny amounts (less than 15% yields) of the desired product, which were just sufficient for a partial characterization, and prompted us to search for a more efficient synthesis of **2**. Since **4** is easily oxidized, the condensation of the preformed octahedral cluster with the Ir(I) complex $[Ir(C_8H_{14})_2Cl]_2$ was tested. The reaction proceeds smoothly at room temperature in CH_3CN, and a complete conversion of $[Fe_6N(CO)_{15}]^{3-}$ into **2** is attained at a molar ratio of $[Ir(C_8H_{14})_2Cl]_2$:**4** = 4. Typical yields are higher than 65%, and this is by far the most convenient reaction for the obtainment of **2**.

Synthesis of $[Fe_4Rh_2N(CO)_{15}]^-$ (3). The monoanion **3** can be prepared in 70% yield by refluxing a CH_3CN suspension of $[Fe_5RhN(CO)_{15}]^{2-}$ and hydrated rhodium chloride, $RhCl_3{\cdot}xH_2O$. Other Rh(I) complexes, such as $[Rh(CO)_2Cl]_2$, were unsuccessfully tested before the Rh(III) salt was found to be much more effective, probably because it allows the formation of Fe(II) according to the equation:

$$[Fe_5RhN(CO)_{15}]^{2-} + RhCl_3 \rightarrow [Fe_4Rh_2N(CO)_{15}]^- + FeCl_2 + Cl^-$$

Instead, lower oxidation states of rhodium imply the formation of iron metal, reducing the driving force of the reaction. The final product is formed selectively in about 3 h and can be recovered by filtration and precipitation from MeOH/water.

Reactivity of the Mixed-Metal Clusters. Clusters **1** and **2** are oxidized by acids without forming any stable hydridic derivatives. Decomposition was also observed after the reaction of **1** with $Au(PPh_3)Cl$ in THF at room temperature. Several attempts were unsuccessfully devoted to the isolation of mixed-metal nitride clusters with higher Rh or Ir contents. However, up to now, we could not characterize any of these product, since analytical and spectroscopic data give contradictory results. The condensation of **2** and $IrCl_3{\cdot}xH_2O$ produces a carbonyl cluster whose IR absorptions (2022 (vs), 1794 (w br) cm^{-1}) exclude the formulation of $[Fe_4Ir_2N(CO)_{15}]^-$; other reproducible reactions under investigation are the condensation of **3** with Rh(−I) and Rh(III) complexes, aimed at the synthesis of the hypothetical compounds $[Fe_3Rh_3N(CO)_{14}]^{2-}$ or $[Fe_3Rh_3N(CO)_{15}]$.

Solid-State Structures. The Molecular Structures of $[Fe_5MN(CO)_{15}]^{2-}$. The crystals of the salts $[PPh_4]_2[Fe_5MN(CO)_{15}]{\cdot}C_4H_8O$ (M = Rh (**1a**) or Ir (**2a**)) are isomorphous, and the two dianions have very similar molecular geometries, with strikingly similar structural parameters. Relevant bond distances and angles are compared in Table 1, and cluster **1** is represented in Figure 1. Cluster **1** consists of an octahedron of metal atoms, lodging a nitrido ligand. Each metal vertex is bound to three carbonyl ligands, but the distribution of terminal and μ-CO differs around rhodium (or iridium) and iron: the d^9 metal atom is bound to two bridging ligands and one terminal ligand; the unique Fe(5) atom trans to the heteroelement has three terminal COs, and the remaining four vertices are bound to two terminal and one μ-CO. Therefore, the excess of one valence electron at the group 9 atom is compensated by the lower connectivity to terminal carbonyls. The electron richness at the Fe(5) center is partially dissipated by semibridging CO(10) with marked deviations from linearity (see Table 1) and Fe(4)···C(10) close contacts of 2.451(6) (**1**) and 2.386(6) Å (**2**). The whole molecules have idealized C_s symmetry, with C(1), N, and C(15) defining the mirror plane; the symmetry of the metal cage is C_{4v}. This architecture can be compared with the even ligand distribution of D_3 symmetry found in the homonuclear **4**, where all iron atoms are equivalent, being bound to one bridging and two terminal COs.[9] The same differences can be also observed in $[Ir_6(CO)_{15}]^{2-}$ [11] and $[Ir_6(CO)_{14}NO]^-$,[12] where the excess electron is brought about by the terminal NO group. On the contrary, the formal substitution of Rh (or Ir) by Fe in octahedral "empty" clusters does not induce ligand reorganization:[6,7]

(8) Alami, M. K.; Dahan, F.; Mathieu, R. *J. Chem. Soc., Dalton Trans.* **1987**, 1983.
(9) Della Pergola, R.; Bandini, C.; Demartin, F.; Diana, E.; Garlaschelli, L.; Stanghellini, P. L.; Zanello, P. *J. Chem. Soc., Dalton Trans.* **1996**, 747.
(10) Zanello, P.; Laschi, F.; Cinquantini, A.; Della Pergola, R.; Garlaschelli, L.; Cucco, M.; Demartin, F.; Spalding, T. R. *Inorg. Chim. Acta* **1994**, *226*, 1.
(11) Demartin, F.; Manassero, M.; Sansoni, M.; Garlaschelli, L.; Martinengo, S.; Canziani, F. *J. Chem. Soc., Chem. Commun.* **1980**, 903.
(12) Della Pergola, R.; Garlaschelli, L.; Manassero, M.; Masciocchi, N. *J. Organomet. Chem.* **1995**, *488*, 199.

Table 1. Selected Interatomic Distances (Å) and Angles (deg) for $[Fe_5RhN(CO)_{15}]^{2-}$ (**1**) and $[Fe_5IrN(CO)_{15}]^{2-}$ (**2**)[a]

	1, M = Rh	**2**, M = Ir
M−Fe(1)	2.875(1)	2.858(1)
M−Fe(2)	2.776(1)	2.767(1)
M−Fe(3)	2.709(1)	2.736(1)
M−Fe(4)	2.689(1)	2.711(1)
Fe(1)−Fe(2)	2.555(1)	2.554(1)
Fe(1)−Fe(4)	2.623(1)	2.643(1)
Fe(1)−Fe(5)	2.648(1)	2.669(1)
Fe(2)−Fe(3)	2.686(1)	2.703(1)
Fe(2)−Fe(5)	2.664(1)	2.677(1)
Fe(3)−Fe(4)	2.727(1)	2.734(1)
Fe(3)−Fe(5)	2.624(1)	2.636(1)
Fe(4)−Fe(5)	2.680(1)	2.700(1)
M−N	2.032(3)	2.048(3)
Fe(1)−N	1.874(3)	1.864(3)
Fe(2)−N	1.862(3)	1.869(4)
Fe(3)−N	1.890(3)	1.913(3)
Fe(4)−N	1.863(3)	1.872(4)
Fe(5)−N	1.878(3)	1.880(3)
M−C(1)	1.848(6)	1.803(7)
M−C(13)	2.066(5)	2.052(6)
M−C(14)	2.112(5)	2.063(6)
Fe(1)−C(2)	1.753(5)	1.750(6)
Fe(1)−C(3)	1.752(5)	1.775(6)
Fe(1)−C(15)	1.949(5)	1.946(6)
Fe(2)−C(4)	1.720(5)	1.726(6)
Fe(2)−C(5)	1.743(6)	1.749(7)
Fe(2)−C(15)	2.014(5)	2.006(6)
Fe(3)−C(6)	1.782(6)	1.778(6)
Fe(3)−C(7)	1.719(6)	1.738(6)
Fe(3)−C(13)	1.952(5)	1.998(6)
Fe(4)−C(8)	1.758(5)	1.759(6)
Fe(4)−C(9)	1.739(6)	1.751(6)
Fe(4)−C(14)	1.915(5)	1.952(6)
Fe(5)−C(10)	1.789(5)	1.811(5)
Fe(5)−C(11)	1.790(6)	1.797(7)
Fe(5)−C(12)	1.734(5)	1.737(6)
$C-O_t$ (average)	1.157	1.147
$C-O_{br}$ (average)	1.172	1.166
M−C(1)−O(1)	175.1(5)	177.2(6)
Fe(5)−C(10)−O(10)	161.9(4)	158.0(5)
$Fe-C_t-O_t$ (average)[b]	174.4	175.0
$M-C_{br}-O_{br}$ (average)	132.6	135.3
$Fe-C_{br}-O_{br}$ (average)	141.5	139.7

[a] Estimated standard deviations are given in parentheses. t = terminal, br = bridging. [b] CO(10) not included.

extended Hückel calculations on model rhodium clusters showed that strong interactions between the interstitial atom and the metal cage are reflected in the stereogeometry of the ligands, leading to carbonyl envelopes of low symmetry.[13]

The Molecular Structure of $[Fe_4Rh_2N(CO)_{15}]^-$. The solid-state structure of **3** was determined for the $[PPh_4][Fe_4Rh_2N(CO)_{15}]$ salt (**3c**). (Labels **c** and **d** refer to different salts of the same monoanion **3**). Two independent anions, labeled **A** and **B** were found in the asymmetric unit. The two anions are, however, very similar, both in the overall geometry and in the structural parameters. One of the clusters is depicted in Figure 2, and the relevant distances and angles are listed in Table 2. Also this cluster is an octahedron of metals, with the two rhodium atoms in *cis* position. The ligand distribution conforms exactly to that described for **1** and **2**: the rhodium atoms have one terminal and two bridging COs, whereas the four iron atoms have either three terminal ligands (Fe(3) and Fe(4), trans to the Rh vertices) or one bridging and two terminal carbonyl groups (Fe(1) and Fe(2)). The carbonyls spanning the Fe−Rh bonds are markedly asymmetric, with Fe−C average distances of 1.90 Å and Rh−C distances of 2.25 Å; on the contrary, CO(13),

(13) Sironi, A. *J. Chem. Soc., Dalton Trans.* **1993**, 173.

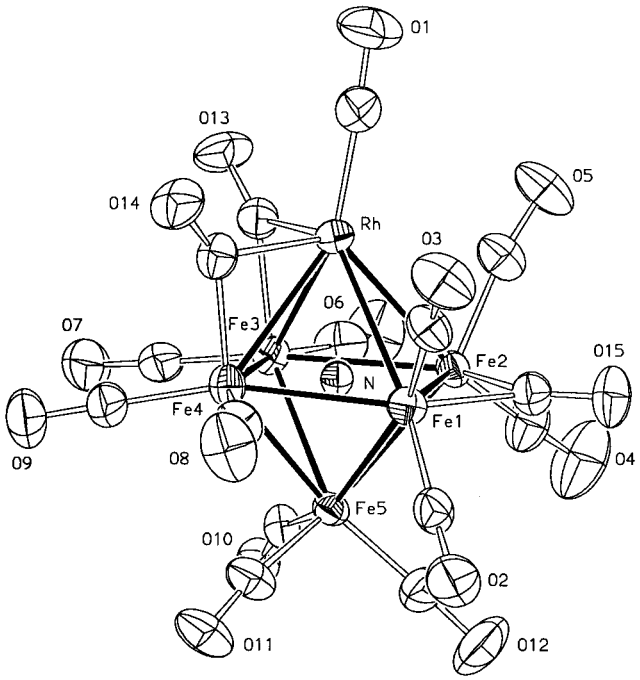

Figure 1. Solid-state structure of the anion $[Fe_5RhN(CO)_{15}]^{2-}$. Ellipsoids are drawn at the 30% probability level. The carbon atoms are labeled as the oxygen to which they are attached.

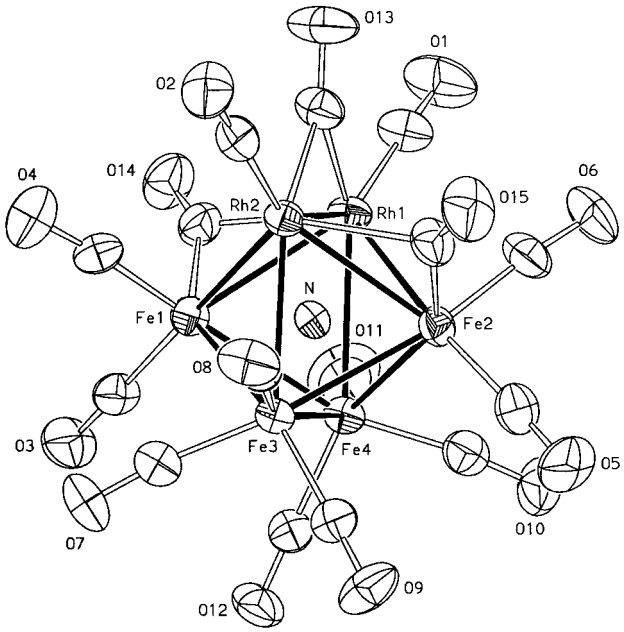

Figure 2. Solid-state structure of the anion $[Fe_4Rh_2N(CO)_{15}]^-$. Ellipsoids are drawn at the 30% probability level. The carbon atoms are labeled as the oxygen to which they are attached.

bridging two rhodium atoms, is symmetric with a Rh−C average bond length of 2.03 Å. Also in **3,** some of the carbonyl groups are not linear, having Fe−C−O angles smaller than 170°; the more marked deviations are shown by CO(8) and CO(10), which can remove electron density from the $Fe(CO)_3$ moieties to which they belong; packing effects can be excluded, since the distortions are comparable in **A** and **B**. Thus, the idealized C_{2v} symmetry of the metal frame is reduced to C_2 by the ligand geometry, with the 2-fold axis passing through the Rh−Rh edge and the interstitial nitride.

It is remarkable that the $[Fe_3Rh_3C(CO)_{15}]^-$ carbide cluster, which can be envisaged as a model of the yet unknown $[Fe_3Rh_3N(CO)_{15}]$, conforms exactly to the same structural pattern:

Table 2. Selected Interatomic Distances (Å) and Angles (deg) for $[Fe_4Rh_2N(CO)_{15}]^-$ (**3**)[a]

	anion **A**	anion **B**
Rh(1)−Rh(2)	2.774(1)	2.775(1)
Rh(1)−Fe(1)	2.720(1)	2.703(1)
Rh(1)−Fe(2)	2.774(1)	2.833(1)
Rh(1)−Fe(4)	2.823(1)	2.831(1)
Rh(2)−Fe(1)	2.825(1)	2.826(1)
Rh(2)−Fe(2)	2.723(1)	2.753(1)
Rh(2)−Fe(3)	2.764(1)	2.756(1)
Fe(1)−Fe(3)	2.657(1)	2. 635(1)
Fe(1)−Fe(4)	2.635(1)	2.621(1)
Fe(2)−Fe(3)	2.660(1)	2.667(1)
Fe(2)−Fe(4)	2.647(1)	2.651(1)
Fe(3)−Fe(4)	2.646(1)	2.634(1)
Rh(1)−N	2.007(4)	2.014(4)
Rh(2)−N	2.011(5)	2.031(4)
Fe(1)−N	1.868(5)	1.899(5)
Fe(2)−N	1.889(5)	1.878(5)
Fe(3)−N	1.877(4)	1.870(4)
Fe(4)−N	1.888(5)	1.861(4)
Rh(1)−C(1)	1.894(8)	1.882(7)
Rh(1)−C(13)	2.044(7)	2.022(8)
Rh(1)−C(14)	2.268(7)	2.275(7)
Rh(2)−C(2)	1.866(7)	1.863(7)
Rh(2)−C(13)	2.046(7)	2.009(8)
Rh(2)−C(15)	2.253(7)	2.191(7)
Fe(1)−C(3)	1.779(7)	1.776(7)
Fe(1)−C(4)	1.777(7)	1.786(6)
Fe(1)−C(14)	1.869(7)	1.867(7)
Fe(2)−C(5)	1.783(8)	1.724(9)
Fe(2)−C(6)	1.780(7)	1.813(7)
Fe(2)−C(15)	1.879(7)	1.978(7)
Fe(3)−C(7)	1.783(7)	1.772(6)
Fe(3)−C(8)	1.823(7)	1.808(6)
Fe(3)−C(9)	1.762(7)	1.753(7)
Fe(4)−C(10)	1.795(8)	1.807(8)
Fe(4)−C(11)	1.803(8)	1.781(7)
Fe(4)−C(12)	1.791(7)	1.780(7)
$C-O_t$ (average)	1.140	1.141
$C-O_{br}$ (average)	1.155	1.157
$M-C_t-O_t$ (average)	173.8	174.0
$Rh-C_{br}-O_{br}$ (average)	132.5	132.8
$Fe-C_{br}-O_{br}$ (average)	150.6	149.1

[a] Estimated standard deviations are given in parentheses. t = terminal, br = bridging.

Table 3. Average Interatomic Distances (Å) in Nitride Clusters **1**−**4**[a]

	1	**2**	**3**	**4**
Fe−M(unbridged)	2.826 (2)	2.813 (2)	2.804 (8)	
Fe−M(bridged)	2.699 (2)	2.724 (2)	2.725 (4)	
Fe−Fe(bridged)	2.555 (1)	2.554 (1)		2.545 (3)
Fe−Fe(unbridged)	2.665 (7)	2.680 (7)	2.645 (10)	2.635 (9)
Rh−Rh			2.775 (2)	
Fe−N	1.873 (5)	1.880 (5)	1.879 (8)	1.864 (6)
M−N	2.032 (1)	2.048 (1)	2.016 (4)	
M−CO(terminal)	1.848 (1)	1.803 (1)	1.876 (4)	
M−CO(bridging)	2.089 (2)	2.058 (2)	2.139 (8)	
Fe−CO(terminal)	1.753 (11)	1.761 (11)	1.784 (20)	1.75 (12)
Fe−CO(bridging)	1.958 (4)	1.976 (4)	1.898 (4)	1.94 (6)
C−O(terminal)	1.157 (12)	1.147 (12)	1.141 (12)	1.15 (12)
C−O(bridging)	1.172 (3)	1.166 (3)	1.156 (3)	1.18 (3)

[a] The number of averaged items is given in parentheses.

the three Rh atoms are arranged in a triangular face, "$Rh_3(\mu\text{-}CO)_3(CO)_3$", and the iron atoms all bear three terminal ligands.[8]

Average metal−metal and metal−N bond lengths in the three nitride clusters are compared in Table 3. The Fe−N average distances in **1**−**3** are strictly comparable to that observed in **4**, whereas the Rh−N mean bond length in the prismatic $[Rh_6N(CO)_{15}]^-$ was 2.130 Å,[14] significantly longer than those reported in the octahedral clusters here. It can be observed that the metal cage of **1** is only slightly compressed if compared to the metal cage of **2**. This is not unexpected, since Rh and Ir have very similar covalent radii. The shortening effect of the bridging ligands on the spanned edges is also relevant, as it was in $[Fe_6N(CO)_{15}]^{3-}$.[9]

^{15}N NMR Spectroscopy. The NMR spectra of the interstitial nitrides were all recorded at room temperature in THF with 20% CD_3CN as the internal standard. The chemical shifts of the ^{15}N ligands were located at $\delta = 470$ ppm in **3** (triplet, $^1J(^{15}N-^{103}Rh) = 8$ Hz), 514 ppm in **1** (doublet, $^1J(^{15}N-^{103}Rh) = 9$ Hz), 514 ppm in **2**, and 560 ppm in **4**,[9] relative to NH_3. The $^{15}N-^{103}Rh$ coupling constants in **1**−**4** are larger than that observed in $[Rh_6N(CO)_{15}]^-$ (6 Hz), in keeping with the shorter Rh−N bond length.[15] Thus, the substitution of a single iron atom by a group 9 atom (either Rh or Ir) displaces the nitride resonance to higher field by 45 ppm. This effect can be largely attributed to the different charges, since it was observed that positively charged ligands (such as H^+ or NO^+) also induce a shift of 20−30 ppm in strictly related nitride compounds.[9,16] The ^{15}N NMR signals of clusters **1**−**4** lie in the typical range for octahedral species (400−600 ppm), and its position is moderately affected by a group 9 atom. Conversely, variations in the geometry of the metal cage, with the resulting loosened Rh−N interactions, has relevant effects on the chemical shift: 108 ppm in the prismatic $[Rh_6N(CO)_{15}]^-$.[15,16] The smooth trend of the chemical shift in anions **1**−**4** cannot be related to the steric compression of the metal cage, as observed for many carbonyl clusters containing interstitial atoms (B, C, N, or O),[17] since the apparent radii of the nitrogen atoms are scattered in a narrow range (r(N) = 0.551 (**1**), 0.558 (**2**), 0.563 (**3**), and 0.558 Å (**4**)). More recently, the chemical shift tensors for exposed and interstitial carbides in carbonyl clusters have been computed by density-functional calculations, in very good agreement with the experimental values. The detailed structural parameters of related nitrido−carbonyl clusters **1**−**4** would possibly be used to check the validity of this approach.[18]

Both the ^{15}N spectrum and the X ray analysis found only one isomer of $[Fe_4Rh_2N(CO)_{15}]^-$, whereas the boride $[Fe_4Rh_2B(CO)_{16}]^-$ exists in two isomers, the *trans* being the most stable. However, in the latter case, the rate of formation of the heterometallic *cis* octahedron was fast in comparison with the *cis* → *trans* isomerization, and the skeletal reorganization could be monitored by ^{11}B NMR from the very beginning of the reaction.[4] On the contrary, the formation of **3** requires a long reaction time at a high temperature, and therefore, only the most stable thermodynamic product could be examined by NMR.

Vibrational Analysis. It is well-known that in vibrational analyses it often proves to be advantageous to work with idealized high-symmetry systems. Descent in symmetry to the real structure then leads to useful predictions or to correct interpretations. Thus, the approach we have used for the study of the vibrations of the cores of the present clusters, together with that of the previously reported $[Fe_6N(CO)_{15}]^{3-}$, starts with the idealized M_6N, octahedral, arrangement.

Metal−Metal Stretching Vibrations. In the O_h point group, the (M−M) modes span the representations A_{1g} (R) + E_g (R) + T_{2g} (R) + T_{1u} (ir) + T_{2u} (inactive). In a simple valence force-field (SVFF) approximation, which usually works as far as the

(14) Bonfichi, R.; Ciani, G.; Sironi, A.; Martinengo, S. *J. Chem. Soc., Dalton Trans.* **1983**, 253.
(15) Martinengo, S.; Ciani, G.; Sironi, A.; Heaton, B. T.; Mason, J. *J. Am. Chem. Soc.* **1979**, *101*, 7095.
(16) Gladfelter, W. L. *Adv. Organomet. Chem.* **1985**, *24*, 41.
(17) Mason, J. *J. Am. Chem. Soc.*, **1991**, *113*, 6056.
(18) Kaupp, M. *J. Chem. Soc., Chem. Commun.* **1996**, 1141.

Table 4. Frequency Values (cm^{-1}) and Assignment of the ν(M−M) Modes[a]

complex	A_{1g}[b]	T_{2g}[b]	E_g[b]	T_{1u}[c]	other[d]
$[Fe_6N(CO)_{15}]^{3-}$	274 (vs)	195 (m)	163 (m w)	ca. 265 (w br)	116 (s br)
$[Fe_5RhN(CO)_{15}]^{2-}$	263 (vs)	190 (m)	166 (m w)	ca. 240 (w br)	109 (s br)
$[Fe_5IrN(CO)_{15}]^{2-}$	262 (vs)	188 (m)	ca. 167 (w br)	ca. 247 (w)	ca. 108 (s br)
$[Fe_4Rh_2N(CO)_{15}]^{-}$	249 (vs)	ca. 202 (w sh), 191 (m), ca. 193 (w)[c]	ca. 178 (w sh), ca. 166 (w br)	ca. 240 (w br)	ca. 118 (m br), 86 (vs br)

[a] The representations refer to the O_h point group (see text). [b] Raman bands (crystals). [c] Infrared bands (CsI or polyethylene discs). [d] Raman bands, presumably belonging to δ(M−M−C) and/or δ(C−M−C).

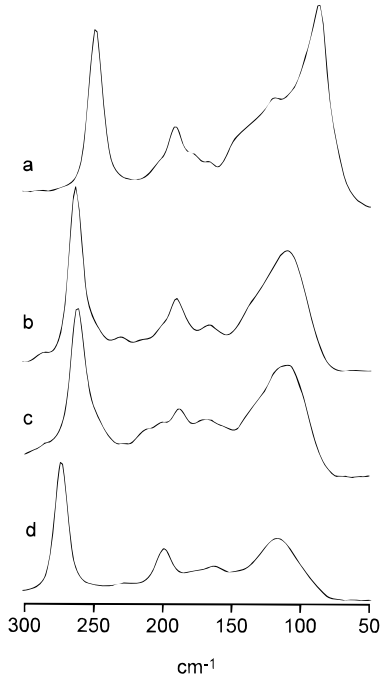

Figure 3. Raman spectra (crystals) of (a) $[Fe_4Rh_2N(CO)_{15}]^-$, (b) $[Fe_5RhN(CO)_{15}]^{2-}$, (c) $[Fe_5IrN(CO)_{15}]^{2-}$, and (d) $[Fe_6N(CO)_{15}]^{3-}$ in the 300−50 cm^{-1} region.

ν(M−M) of metal clusters are concerned,[19] the difference in the mode frequencies is determined by the *G* matrix elements, the only non-zero *F* matrix element being the metal−metal stretching force constant. Thus, the expected frequency ratios are $2:\sqrt{3}:\sqrt{2}:1$ (A_{1g}:T_{1u}:T_{2g}:E_g).

The $[Fe_6N(CO)_{15}]^{3-}$ Cluster. The structure of this cluster has been recently described[9] and consists of a quasi octahedral metal core, where three edge-bridging CO groups lead to a shortening of the corresponding M−M distances, giving rise to a D_3 symmetry. Descent in symmetry from O_h to D_3 transforms A_{1g} into A_1, E_g into E, T_{2g} into $A_1 + E$, and T_{1u} into $A_2 + E$, where A_1 species are Raman active, A_2 infrared active, and E both Raman and infrared active. The splitting of the triply-degenerate modes results from force constant perturbations,[20] if two, at least, different force constant values are assumed, f_b for the bridged M−M bonds and *f* for the unbridged (the M−M distances are so close that we have used a single value only, although D_3 symmetry requires two independent unbridged M−M groups and, in principle, two different *f* values). However, such a calculation requires that $F(T_{2g})$ remains a constant matrix and that the splitting could be only observed in the T_{1u} vibration.[20]

Figure 3 illustrates the Raman spectrum of this complex in the (M−M) region (together with the spectra of the other complexes), and Table 4 reports the frequency values and the suggested assignments.

The very strong Raman band at 274 cm^{-1} is undoubtedly the A_1 (previously A_{1g}) totally symmetric mode. The T_{2g}-derived modes, expected as uniquely Raman active according to the above arguments, are assigned to the strong band at 194 cm^{-1}; this assignment is supported by the frequency ratio with the A_1 mode: calculated = 1.41, found = 1.41. The next medium Raman band at lower frequency is presumably the E (previously E_g) mode. The frequency ratio is not far from the expected value, 1.7 instead of 2, the shift probably being due to coupling with the skeletal modes (δ(Fe−Fe−C) and/or δ-(C−Fe−C)), which are included in the broad and strong absorption at 109 cm^{-1}.

Infrared activity is expected for the T_{1u}-derived A_2 and E modes, but the band intensity is presumably low because of the small change of the dipole moment associated with the metal−metal stretching. Only a weak feature is evident at ca. 265 cm^{-1} in the low-temperature spectrum. As the frequency is higher than that expected on the basis of the frequency ratio (ca. 240 cm^{-1} is predicted), the band may be tentatively assigned to the E mode, because this mode can be "pushed up" by the coupling with the other E mode at 167 cm^{-1}.

$[Fe_5MN(CO)_{15}]^{2-}$ Clusters. The real symmetry of the metal cores of these complexes is C_s, as reported above; so, all the degenerancies of the modes are expected to be lost, giving seven A′ and five A″ species; complex spectral patterns are expected. Surprisingly, the Raman spectra of both of the complexes are simple and very similar to that of the iron cluster (see Figure 3): the infrared spectra are much less informative and show only a weak and broad band.

To explain this behavior, we may assume that the main perturbation is given by the difference in metal atom masses and that the shortening of metal−metal bond distances due to the bridging CO groups does not introduce a significant variation in force constant. The ideal symmetry is C_{4v}, and the modes transform as follows: A_{1g} into A_1, E_g into $A_1 + B_1$, T_{2g} into $B_2 + E$, and T_{1u} into $A_1 + E$. The effect of this perturbation has been calculated[20] and affects both the *G* matrix (different atomic masses) and F matrix elements (different force constant values due to different atoms: *f*′, the Fe−M stretching force constant, is probably greater than *f*, the Fe−Fe stretching force constant).

In this light, the T_{2g} mode is expected to split under C_{4v} symmetry but the *F* and *G* matrices have the opposite effect on the two derived modes, *F* giving rise to $\nu(E) > \nu(B_2)$ and *G* giving rise to $\nu(B_2) > \nu(E)$ (the values are $F(B_2) = f$, $G(B_2) = 2/m_{Fe}$, $F(E) = (f + f')/2$, $G(E) = {}^1/_2\,(3/m_{Fe} + 1/m_{Rh(Ir)})$), so the splitting is not evident. Incidentally, the casual coincidence between ν(E) and $\nu(B_2)$ allows an estimation of the relationship between *f* and *f*′ and gives $f \cong 0.8f'$ (Rh) and $f \cong 0.7f'$ (Ir). The splitting of the T_{1u} and E_g modes has a contribution from both the *F* and *G* matrices. The weakness and the broadness of the bands prevent a clear observation: the Raman spectrum of the Ir complex only shows an incipient splitting of the E_g band. So the apparent "octahedral" behavior of the spectral patterns is clear and the assignment of the modes, as reported in Table 4, has been made accordingly.

The $[Fe_4Rh_2N(CO)_{15}]^-$ Cluster. Again, the further lowering of the symmetry does not significantly affect the spectral patterns. The Raman spectrum is dominated by the two bands

(19) Spiro, T. G. *Prog. Inorg. Chem.* **1970**, *11*, 1.
(20) Creighton, J. A. *Inorg. Chem.* **1982**, *21*, 1.

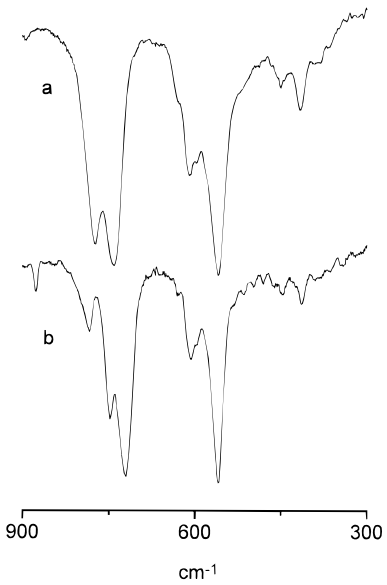

Figure 4. Infrared spectra (CsI disc) of (a) $[NEt_4]_2[Fe_5Ir^{14}N(CO)_{15}]$ and (b) $[NEt_4]_2[Fe_5Ir^{15}N(CO)_{15}]$ in the 900−300 cm^{-1} region.

at 249 and 191 cm^{-1}, presumably derived from the "octahedral" A_{1g} and T_{2g} modes. The E_g-derived modes give rise to a weak and broad band in the usual range. The low symmetry of the cluster is probably pointed out by the appearance of weak features at ca. 178 and 202 cm^{-1}. The infrared spectrum shows, as usual, a broad absorption at ca. 240 cm^{-1} (T_{1u}-derived modes).

It is interesting to observe that the frequency order of the totally symmetric mode is Fe_6N > $Fe_5RhN \cong Fe_5IrN$ > Fe_4Rh_2N; this order clearly depends on the differences of both the atomic masses and the force constants. Using the appropriate *G* matrix for each complex, an "average" cluster force constant can be calculated: it is 62 N/m for both Fe_6N and Fe_5RhN, 64 N/m for Fe_5IrN, and 60 N/m for Fe_4Rh_2N. The closeness of the values results from a balance between the values of force constants, bond distances, and cluster charges and may suggest that the potential energy holding the metal atoms of the cage is roughly the same.

Metal-Nitrogen Stretching Vibrations. These vibrations are expected in the 800−650 cm^{-1} region, a region which is partially obscured by strong infrared absorptions of the $[P(C_6H_5)_4]^+$ counterion. For a reliable assignment, we attempted to crystallize the tetraethylammonium salt, where the counterion is "transparent" below 780 cm^{-1}. We succeeded with the Ir compound, because its synthesis does not require the use of the large phosphonium cation (see Experimental Section).

The $[Fe_5MN(CO)_{15}]^{2-}$ Cluster. In octahedral symmetry, the ν(M−N) span a unique infrared-active T_{1u} mode. If the real symmetry of the $[Fe_5MN(CO)_{15}]^{2-}$ complexes approaches C_{4v}, this T_{1u}mode splits into $A_1 + E$, which are expected to give rise to strong infrared and weak Raman bands. In fact, the Raman spectrum of $[N(C_2H_5)_4]_2[Fe_5IrN(CO)_{15}]$ does not show any significant feature assignable to these modes, whereas the infrared spectrum (Figure 4a) clearly shows two strong bands at 773 and 740 cm^{-1}. In the spectrum of the ^{15}N isotopomer, they are shifted to 747 and 721 cm^{-1}, respectively (Figure 4b), so the assignment is straightforward. Their form and relevant intensities indicate the highest frequency band to be the A_1 mode. This analysis allows an unambiguous assignment of the ν(M−N) modes of the $[P(C_6H_5)_4]_2[Fe_5MN(CO)_{15}]$ salts, even though they are partially obscured by the absorptions of the cations (Table 5). In a simple valence force-field approximation, the *F*(E) matrix depends on the Fe−N stretching force constant

Table 5. Frequency Values (cm^{-1}) of M−N Stretching Vibrations

	$[N(C_2H_5)_4]^+$				$[P(C_6H_5)_4]^+$			
	^{14}N		^{15}N		^{14}N		^{15}N	
	room temperature	110 K	room temperature	110 K	room temperature	110 K	room temperature	110 K
$[Fe_5RhN(CO)_{15}]^{2-}$	775 (m), 744 (m)	784 (m), 754 (m), 744 (m)	747 (m), 721 (m)	758 (m), 732 (m sh), 724 (m)	769 (m), 750 (m)	780 (m), 753 (m)	745 (m br)[a]	755 (m), 733 (sh)
$[Fe_5IrN(CO)_{15}]^{2-}$	744 (m), 722 (m)	756 (m), 737 (m), 722 (m)			771 (m), 743 (m)	780 (m), 750 (m)	745 (m)[a]	754 (m)[a]

[a] Obscured by the absorption of the cation.

only: its value can be easily calculated as ca. 204 N/m for both of the clusters. As a consequence, $\nu(A_1)$ allows the calculation of the M−N stretching force constants, which are ca. 242 N/m for Rh and ca. 253 N/m for Ir. These values are quite surprising, because the M−N stretching force constant decreases moving down the transition series:[21] see later discussions.

The $[Fe_4Rh_2N(CO)_{15}]^-$ Cluster. The idealized symmetry of the core is C_{2v}, so three different modes, A_1, B_1, and B_2, are expected for the metal−nitrogen vibrations. The A_1 and B_1 modes are related to the motion of the N atom in the Fe_2Rh_2 plane and the B_2 mode to the motion along the axis perpendicular to this plane: the former modes have both Fe−N and Rh−N stretching character; the latter one has Fe−N stretching character only. The SVFF model easily gives $\nu(A_1) = \nu(B_1)$ > or < $\nu(B_2)$, depending on if f(Rh−N) is greater or less than f(Fe−N). Two bands are evident in the infrared spectrum at 744 and 722 cm^{-1}. The last one, clearly split at low temperature, is undoubtedly assigned to both the A_1 and B_1 modes. The calculated values of the M−N stretching force constant are ca. 200 N/m for Fe and ca. 190 N/m for Rh, according to literature data.[21]

A comparison with the other clusters of this series show an increase of f(Fe−N) in the order Fe_6N > Fe_5RhN > Fe_4Rh_2N, which is the order of the charge of the clusters. This trend could be ascribed to the increase of the repulsion between the strongly electronegative N atom and the metal cage, as the negative charge on the cage increases. In this light, we can explain the "anomalous" values of f(M−N) of the $[Fe_5MN(CO)_{15}]^{2-}$ complexes. We suspect a charge effect too, as the negative charge could be preferentially localized on the more electronegative metal, which is Rh (or Ir) with respect to Fe, according to their electron affinities.[22] This effect is clearly larger in $[Fe_5MN(CO)_{15}]^{2-}$ than in $[Fe_4Rh_2N(CO)_{15}]^-$ and accounts for the different f(Rh−N) values.

C−O Stretching Vibrations. The frequencies of the absorptions for the terminal COs in **1**, **2**, and **3** ($[Fe_5RhN(CO)_{15}]^{2-}$ 1954 cm^{-1}; $[Fe_5IrN(CO)_{15}]^{2-}$ 1953 cm^{-1}; $[Fe_4Rh_2N(CO)_{15}]^-$ 2008 cm^{-1}), compared with those of Fe−Rh or Fe−Ir clusters with the same metal/charge ratio,[6,7] show a significant shift to lower wavenumbers. This effect can be attributed to the strong π-donor ability of the nitride,[23] which can be coupled with the π*-acidity of the carbonyl ligands, and is comparable to that of a full negative charge.

Our recent papers deal with the correlation between the ν(CO) features and the geometry of the carbonyl clusters. The significant difference between the ν(CO) vibrational patterns of terminal and bridging CO groups has been recognized, the first substantially invariant with respect to the molecular geometry[24] and the second strongly dependent on it.[25] The spectra of the present clusters are easily explained on the basis of the proposed models.

Terminal CO Groups. The terminal ν(CO) patterns have been explained on the basis of Stone's tensor harmonic approach to the bond in cluster compounds.[26] Spectroscopic models have been developed for the homonuclear metal carbonyl clusters only[24] and may be applied in the present case to the $[Fe_6N(CO)_{15}]^{3-}$ compound. Its infrared spectrum in CH_3CN solution shows a single strong absorption at 1914 cm^{-1},[9] and the Raman spectrum in the solid state is basically characterized by two features, a medium sharp band at 1986 cm^{-1} and a strong and broad band centred at 1875 cm^{-1}. The simplest model, which assumes a pseudospherical arrangement of the terminal ν(CO) vectors attached to the metal atoms, predicts for the 12 terminal ν(CO)s a totally symmetric S mode at the highest energy followed, in the order of decreasing energy, by a P mode (3-fold degenerate), a D mode (5-fold degenerate), and an F mode (3-fold degenerate). The S and D modes will be Raman allowed and the P mode infrared allowed; the F mode is not dipolar and must be silent. So, the predicted spectral pattern may consist of a single infrared band and two Raman bands, one on either side of the infrared: this is exactly what has been observed.

Table 6. Frequency Values (cm^{-1}) of Bridging C−O Stretching Vibrations

complex	infrared[a]	Raman[b]
$[Fe_6N(CO)_{15}]^{3-}$	1740 (m)	1743 (m), 1754 (m sh)
$[Fe_5RhN(CO)_{15}]^{2-}$	1815 (w, br)	1810 (m), 1795 (m)
$[Fe_5IrN(CO)_{15}]^{2-}$	1794 (m)	ca. 1790 (m br)
$[Fe_4Rh_2N(CO)_{15}]^-$	1860 (m br), 1860 (m br),[c] 1818 (m)[c]	1895 (w), 1875 (w), 1836 (w)

[a] CH_3CN solution. [b] Crystals. [c] CsI disc.

Bridging CO Groups. A quite general approach to the interpretation of the bridging ν(CO) spectra indicates that the form of the spectra is determined by the geometrical disposition of the CO groups, with minor effects due to the metal atom framework.[25] The three bridging carbonyl ligands in $[Fe_5RhN(CO)_{15}]^{2-}$ and $[Fe_5IrN(CO)_{15}]^{2-}$ clusters are not related by a C_3 axis, as in $[Fe_6N(CO)_{15}]^{3-}$, nonetheless the bridging COs lie at the corner of a quasiequilateral triangle and have the vibrational behavior dictated by the local D_{3h} symmetry.[27] The model predicts a nondegenerate A mode and a doubly-degenerate E mode for their vibrations. The spectral patterns should consist of an infrared band (E) and two Raman bands (A + E), with one coincident. The spectra show the predicted behavior (Table 6), despite the low symmetries of the metal cores that do not allow it to maintain the C_3 axis. The $[Fe_4Rh_2N(CO)_{15}]^-$ cluster does not fulfill this simple model, as shown by the spectra reported in Figure 5. Several structural peculiarities (two independent molecules in the unit cell, a marked asymmetry of the COs bridging the Fe−Rh bonds, the semibridging character of some terminal COs) can be advanced to explain the "anomalies" of the solid-state spectra. Remarkable in this light is the difference between the infrared spectra in solution (a broad band at ca. 1860 cm^{-1}) and in the solid state (a broad band at ca 1860 cm^{-1} plus a sharp one at 1818 cm^{-1}). This peculiar pattern resembles that reported for $Co_6C_2S(CO)_{12}$[28] and similarly suggests a CO-bridged system in which one "regular" bridge ($(\mu$-CO)Rh_2) gives rise to a "normal" band and some other bonds, with different symmetries, that merge into a broad band. In solution, the broadness of the unique band may arise from a sort of fast fluctional mechanism between all the bridging COs.

Electrochemistry and Coupled EPR Measurements. Figure 6, which refers to $[Fe_5RhN(CO)_{15}]^{2-}$, shows the typical cyclic voltammetric response exhibited by the dianions $[Fe_5MN(CO)_{15}]^{2-}$ (M = Rh, Ir) in tetrahydrofuran solution.

(21) Creighton, J. A.; Della Pergola, R; Heaton, B. T.; Martinengo, S; Strona, L.; Willis, D. A. *J. Chem. Soc., Chem. Commun.* **1982**, 864.
(22) Emsley, J. *The Elements*; Clarendon Press: Oxford, 1989.
(23) (a) Greenwood, N. N.; Earnshaw, A. *The Chemistry of the Elements*; Pergamon Press: Oxford, 1989, p 480. (b) Griffith,W. P. *Coord. Chem. Rev.* **1972**, *8*, 369.
(24) Kettle, S. F. A.; Diana, E.; Rossetti, R.; Stanghellini, P. L. *J. Am. Chem. Soc.*, in press.
(25) Kettle, S. F. A.; Diana, E.; Rossetti, R.; Stanghellini, P. L.; Della Pergola, R; Garlaschelli, L. *Inorg. Chim. Acta* **1994**, *227*, 241.
(26) Stone, A. J. *Inorg. Chem.* **1981**, *20*, 563.
(27) Kettle, S. F. A.; Diana, E.; Stanghellini, P. L.; Della Pergola, R.; Fumagalli, A. *Inorg. Chim. Acta* **1995**, *235*, 407.
(28) Gervasio, G.; Rossetti, R.; Stanghellini, P. L.; Bor, G. *Inorg. Chem.* **1984**, *23*, 2073.

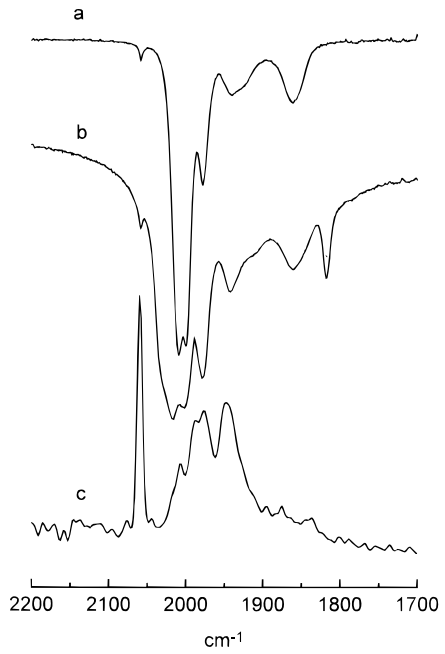

Figure 5. Infrared spectra of $[Fe_4Rh_2N(CO)_{15}]^-$ in the CO stretching region in (a) THF solution and (b) CsI disc and (c) the Raman spectrum (crystals).

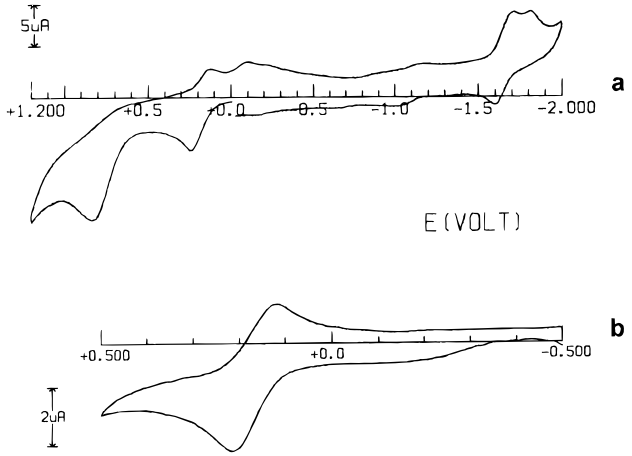

Figure 6. Cyclic voltammograms recorded at a platinum electrode on a THF solution containing $[PPh_4]_2[Fe_5RhN(CO)_{15}]$ (4×10^{-4} mol dm^{-3}) and $[NBu_4][PF_6]$ (0.2 mol dm^{-3}). Scan rate = (a) 0.2 V s^{-1}, (b) 0.05 V s^{-1}.

In both cases, the first anodic step and the reduction process possess features of partial chemical reversibility whereas the second anodic step is irreversible in character. Controlled potential coulometric tests corresponding to the first oxidation process ($E_w = +0.4$ V) show that the current tends to slow down after 1 electron/molecule but it remains higher than the residual current up to the overall consumption of 2 electrons/molecule. The fact that a rather complex electrode mechanism takes place is also verified by the analysis of the cyclic voltammograms with scan rate.[29] As a matter of fact, for $[Fe_5RhN(CO)_{15}]^{2-}$, the progressive increase of the scan rate from 0.02 to 1.00 V s^{-1} causes the peak current ratio i_{p_c}/i_{p_a} to decrease slightly from 0.80 to 0.74, for $[Fe_5IrN(CO)_{15}]^{2-}$ the ratio remains almost unchanged at 0.67. Taking into account that, as discussed below, the paramagnetic monoanions $[Fe_5MN(CO)_{15}]^-$ can be successfully electrogenerated by electrolysis at low temperature (−20 °C), we assume that, in spite of the long times of macroelectrolysis, an ECE mechanism is likely operative; in the cyclic voltammetric time scale, the following E_rC_r mechanism can explain the trend in peak current ratio with scan rate v:

$$[Fe_5MN(CO)_{15}]^{2-} \underset{+e^-}{\overset{-e^-}{\rightleftharpoons}} [Fe_5MN(CO)_{15}]^-$$

$$[Fe_5MN(CO)_{15}]^- \underset{k_b}{\overset{k_f}{\rightleftharpoons}} \text{unknown product}$$

Here $k_f + k_b \approx nFv/RT$.[29]

At present, we have no chemical information about the nature of the reorganization product of the $[Fe_5MN(CO)_{15}]^-$ monoanions; however, cyclic voltammetry on solutions from exhaustive electrolysis at room temperature corresponding to the first oxidation of the two complexes points out the presence of a reversible reduction at $E^{\circ\prime} \approx -1$ V, well matching that of $[Fe_5N(CO)_{14}]^-$.[30] Such a peak system is somewhat detectable in Figure 6a in the backscan after traversing the second anodic step. In this connection, we recall that the three-electron oxidation of $[Fe_6N(CO)_{15}]^{3-}$ also ultimately generates $[Fe_5N(CO)_{14}]^-$.[9] From a speculative viewpoint, the instantaneously electrogenerated monoanion $[Fe_5MN(CO)_{15}]^-$ could slowly tend to be in equilibrium with the fragment $[Fe_5N(CO)_{14}]^-$.

Because of the chemical complications accompanying either the second oxidation or the reduction process, we have not studied these processes further. On the basis of their relative peak heights in the cyclic voltammetry, we assign them to primary two-electron and one-electron steps, respectively. We underline that the cathodic process cannot be assigned to the reduction of the $[PPh_4]^+$ countercation in that this reduces at notably more negative potential values.[31] Table 7 compiles the electrochemical parameters of the discussed redox changes.

In view of the relative stability of the monoanions $[Fe_5MN(CO)_{15}]^-$, we decided to study their EPR paramagnetism. In order to slow down their degradation rate further, they were electrogenerated by controlled potential electrolysis at −20 °C.

Figure 7a shows the X-band EPR spectrum recorded at liquid nitrogen temperature ($T = 100$ K) of the electrogenerated monoanion $[Fe_5IrN(CO)_{15}]^-$. The line shape is typical of an $S = {}^1/_2$ paramagnetic species displaying significant metal-in character ($g_i > g_e = 2.0023$; $\delta H_i \geq 10$ G).

The spectral analysis is suitably carried out in terms of an $S = {}^1/_2$ rhombic Hamiltonian. The paramagnetic parameters are as follows: $g_l = 2.230(4)$; $g_m = 2.066(4)$; $g_h = 2.048(4)$; $\langle g \rangle = 2.133(4)$. The strongly metal-based rhombic absorption suggests that the unpaired electron is distributed over the whole metal frame of the distorted octahedral assembly.

The best way to simulate the experimental spectrum[32] was obtained assuming that the unpaired electron magnetically interacts with the interstitial nitrogen nucleus (I = 1) rather than

Table 7. Electrochemical Characteristics of the Redox Changes Exhibited by $[Fe_5MN(CO)_{15}]^{2-}$ in THF Solution at 20 °C

M	$E_{p+/-}$[a] (V)	$E^{\circ\prime}_{-/2-}$ (V)	ΔE_p[a] (mV)	$t_{1/2(\text{monoanion})}$ (s)	$E^{\circ\prime}_{2-/3-}$ (V)	ΔE_p[a] (mV)
Rh	+0.77	+0.19	123	∼20	−1.63	95
Ir	+0.80	+0.14	130	∼15	−1.58	98

[a] Measured at 0.1 V s^{-1}.

(29) Brown, E. R.; Sandifer, J. R. Cyclic voltammetry, A. C. polarography and related techniques. *Physical Methods of Chemistry*; Weissberger, A., Rossiter, B. W., Eds.; Wiley Interscience: New York, 1986; Vol. 2.

(30) Hourihane, R.; R. Spalding, R.; Ferguson, G.; Deeney, T.; Zanello, P. *J. Chem. Soc., Dalton Trans.* **1993**, 43.

(31) Wei, C.-H.; Bockman, T. M.; Kochi, J. K. *J. Organomet. Chem.* **1992**, *428*, 85.

(32) Lozos, J. P.; Hoffman, B. M.; Franz, C. G. *QCPE* **1973**, *243*, 11.

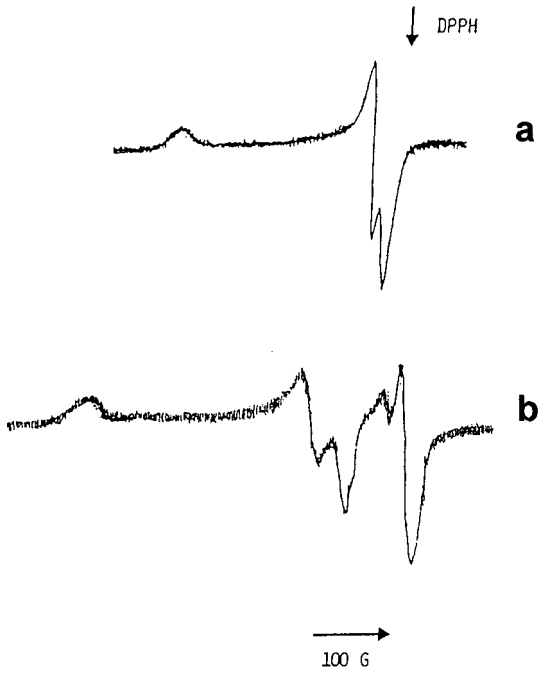

Figure 7. X-band EPR spectra of the electrogenerated monoanion $[Fe_5MN(CO)_{15}]^-$ in THF solution, $T = 100$ K, (a) M = Ir, (b) M = Rh.

with the two iridium isotopes (I−Ir(191,193) = $^3/_2$; 100% of natural abundance). On this basis, the following anisotropic splittings have been calculated: $a_{l(N)} = 8(2)$ G; $a_{m(N)} = 3(2)$ G; $a_{h(N)} = 4(2)$ G $\langle a\rangle_{(N)} = 5(2)$ G. Raising the temperature induces a decrease of the spectral intensity, and at the glassy−fluid transition, the paramagnetic signal drops out as a consequence of effective fastening of the electron relaxation rates induced by temperature. In agreement with the incomplete stability of the radical monoanion, refreezing the solution partially restores the previous anisotropic spectrum.

Figure 7b shows the liquid nitrogen X-band EPR spectrum recorded on a solution resulting from the anodic oxidation of $[Fe_5RhN(CO)_{15}]^{2-}$. The complex line shape arises from two overlapping S = 1/2 paramagnetic species (in a molar ratio of ∼4:1), both displaying resolved anisotropic features. The low-field, major component exhibits a rhombic pattern ($g_i > g_e = 2.0023$; $\Delta H_i \geq 18(2)$ G) with strong metal-in character and paramagnetic parameters reminiscent of the previous monoanion $[Fe_5IrN(CO)_{15}]^-$: $g_l = 2.281(5)$; $g_m = 2.078(5)$; $g_h = 2.046(5)$; $\langle g\rangle = 2.135(5)$. Therefore, we assign it to the primarily electrogenerated monoanion $[Fe_5RhN(CO)_{15}]^-$; the pronounced anisotropic features likely reflect an increased distortion of the overall metal framework with respect to the iridium analog.

The high-field axial spectrum of the minor component ($g_{\|} = 2.018(5)$; $g_\perp$ 1.995(5); $\langle g\rangle = 2.003(5)$) is assigned to a degradation byproduct. On the basis of the best fit simulation procedures, an upper limit for the magnetic interaction of the unpaired electron with the nitrogen nucleus can be proposed: $a_{l(N)} = 8(2)$ G; $a_{m(N)} = 5(2)$ G; $a_{h(N)} = 2(2)$ G $\langle a\rangle_{(N)} = 5(2)$ G. Coupling with the Rh nucleus (I−Rh(103) = $^1/_2$; 100% natural abundance) affords a bad fit between the experimental and simulated spectra.

Raising the temperature induces a drastic decrease of the spectral intensity, and at the glassy−fluid transition, both of the paramagnetic signals disappear. Refreezing the solution partially restores the overall spectrum.

Figure 8 shows that, at variance with the preceding dianions, the dirhodium monoanion $[Fe_4Rh_2N(CO)_{15}]^-$ undergoes a first-reduction process ($E^{o\prime} = -0.88$ V) having a partially chemically

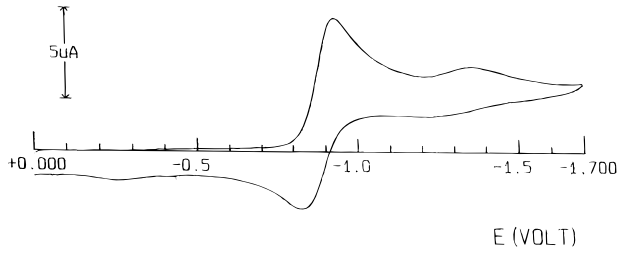

Figure 8. Cyclic voltammogram recorded at a platinum electrode on a THF solution containing $[Fe_4Rh_2N(CO)_{15}][NEt_4]$ (6×10^{-4} mol dm^{-3}) and $[NBu_4][PF_6]$ (0.2 mol dm^{-3}). Scan rate = 0.05 V s^{-1}.

reversible character (for instance, at 0.05 V s^{-1}, $i_{p(backward)}/i_{p(foreward)} = 0.75$; $\Delta E_p = 120$ mV), followed by a second minor irreversible peak (E_p −1.36 V).

Controlled potential coulometry in correspondence to the first reduction ($E_w = -1.0$ V) indicates the consumption of 2 electrons/molecule. Simply based on the following EPR measurements we assume an EEC mechanism to be operative.

We have not studied in detail the second reduction process in that analysis of the cyclic voltammetric responses shows it to be due to an adsorption process (i_{p_c} linearly increases with scan rate).

Samples from the two-electron reduction of $[Fe_4Rh_2N(CO)_{15}]^-$ exhibit unresolved, anisotropic, and very broad EPR signals both at liquid nitrogen and fluid solution temperatures. Very minor metal-in character byproducts can be also observed in both the glassy and fluid solutions.

The paramagnetic parameters of the main absorption are $g_{averaged(100K)} = 2.36$; $\Delta H_{averaged(100K)} = 1150$ G; $g_{averaged(300K)} = 2.26$; $\Delta H_{averaged(300K)} = 875$ G. The line shape analysis is consistent with a paramagnetic species in a triplet state ($S = 1$) in which the two unpaired electrons are localized on the same degenerate molecular orbital. A large zero-field splitting term may account for the EPR parameters of the trianion $[Fe_4Rh_2N(CO)_{15}]^{3-}$.[33] Increasing the temperature induces reversible line-narrowing, likely due to an effective lowering of the structural anisotropies; on the other hand, the refrozen solution completely restores the glassy spectrum.

Hydroformylation. Clusters containing interstitial atoms or main group bridging ligands are typically resistant toward degradation. Therefore, compounds of this kind are considered the most interesting candidates to verify catalysis *via* clusters.[34] In this context, the carbide $[Fe_5RhC(CO)_{16}]^-$ was used for the hydroformylation of 1-pentene. It showed a only moderate activity, and it was transformed into two different, previously unknown, carbide clusters, $[Fe_4Rh_2C(CO)_{16}]$ and $[Fe_3Rh_3C(CO)_{15}]^-$.[8]

A comparison of the stability of Fe−Rh carbide and nitride in forcing conditions can be taken as a measure of the relative stability of the bond between the metal cage and interstitial atom. Therefore, the nitride clusters **1** and **3** were subjected to the same catalytic experiment, although the difficulty in their preparation prevented a systematic investigation. Moreover, we were looking for some evidence of new compounds, which we could not obtain by standard chemical reactions.

The dianion $[Fe_5RhN(CO)_{15}]^{2-}$ was the most resistant toward fragmentation, and the last traces of unreacted compound disappeared after 4 h; the infrared of the final solution showed the presence of $[Fe_4N(CO)_{12}]^-$ only; no rhodium containing species could be isolated in the reaction mixture. The conver-

(33) Mabbs, F. E.; Collison, D. *Electron Paramagnetic Resonance of d Transition Metal Compounds*; Elsevier: Amsterdam, 1992.
(34) (a) Süss-Fink, G.; Meister, G. *Adv. Organomet. Chem.* **1993**, *35*, 41. (b) Vidal, J. L.; Walker,W. E. *Inorg. Chem.* **1980**, *19*, 896.

Table 8. Crystallographic Data and Intensity Collection Parameters for Compounds **1a**, **2a**, and **3c**

	1a	**2a**	**3c**
formula	$C_{67}H_{48}Fe_5NO_{16}P_2Rh$	$C_{67}H_{48}Fe_5IrNO_{16}P_2$	$C_{39}H_{20}Fe_4NO_{15}PRh_2$
fw	1567.21	1656.51	1202.76
space group	$P\bar{1}$ (No. 2)	$P\bar{1}$ (No. 2)	$P2_1$ (No. 4)
a, Å	11.894(2)	11.906(1)	13.557(2)
b, Å	12.551(3)	12.511(2)	20.031(2)
c, Å	23.289(4)	23.375(2)	15.983(2)
α, deg	90.54(2)	90.45(1)	
β, deg	94.01(2)	94.06(1)	91.25(1)
γ, deg	106.10(2)	106.25(1)	
V, Å^3	3330.6(1.3)	3333.0(7)	4339.3(9)
Z	2	2	4
D_{calcd}, g cm^{-3}	1.563	1.650	1.841
μ(Mo Kα), cm^{-1}	14.1	31.5	21.4
final R and R_w indices[a]	0.039, 0.053	0.035, 0.049	0.035, 0.048

[a] $R = [\sum(|F_o - k|F_c||)/\sum F_o]$; $R_w = [\sum w(F_o - k|F_c|)^2/\sum wF_o^2]^{1/2}$. $w = 1/(\sigma(F_o))^2$, $\sigma(F_o) = [\sigma^2(I) + (pI)^2]^{1/2}/2F_oL_p$, and p (the ignorance factor) = 0.06 for **1a** and **2a** and 0.05 for **3c**.

sion of 1-pentene was about 10%, corresponding to a TOF (turnover frequency) of 0.44 min^{-1}. The selectivity in *n*-hexanal was 66%.

The monoanion $[Fe_4Rh_2N(CO)_{15}]^-$ was much more active, and after 2 h it had completely reacted. The final product of decomposition was a brown residue, soluble in CH_3CN, which could not be characterized. Its infrared spectrum and its chemical properties suggested that a rhodium-rich, high-nuclearity cluster was formed.[35] The conversion of 1-pentene was higher than 70%, corresponding to a TOF of 5.85 min^{-1}. The branched aldehyde was formed preferentially in this case, and the selectivity in *n*-hexanal dropped to 36%.

Both experiments strongly suggest that the reconstruction of a metal cage around the nitride ligand is less favored that around the carbide[8] and that rhodium fragments of low nuclearity are generated in solution and are likely responsible for the catalytic activity.

Experimental Section

All of the solvents were purified and dried by conventional methods and stored under nitrogen. All of the reactions were carried out under an oxygen-free nitrogen atmosphere using the Schlenk-tube technique.[36] $[NEt_4][Fe_4N(CO)_{12}]$,[37] $[PPh_4][Rh(CO)_4]$,[38] $[Ir(C_8H_{14})_2Cl]_2$,[39] and $[NEt_4]_3[Fe_6N(CO)_{15}]$[9] were prepared by literature methods. Infrared spectra in solution were recorded on a Perkin-Elmer 16 PC FT-IR spectrophotometer, using calcium fluoride cells previously purged with N_2. Solid-state infrared spectra were recorded in CsI pellets using a Perkin−Elmer model 580 spectrophotometer. Raman spectra were recorded on the crystals with a Bruker RFS 100, with a Nd-YAG laser and a Ge-diode detector (laser power 50 mW, resolution 4 cm^{-1}). Elemental analyses were carried out by the staff of Laboratorio di Analisi of the Dipartimento di Chimica Inorganica, Metallorganica e Analitica. ^{15}N NMR spectra were recorded on a Bruker AC200 spectrometer operating at 20.28 MHz. The spectra are reported in ppm downfield from the external standards (NH_3 for ^{15}N).

The materials and apparatus for the electrochemistry and coupled EPR measurements have been described elsewhere.[40] All of the potential values are referenced to the saturated calomel electrode (SCE). Under the present experimental conditions, the one-electron oxidation of ferrocene occurs at +0.52 V.

Synthesis of $[PPh_4]_2[Fe_5RhN(CO)_{15}]$ (1a). $[NEt_4][Fe_4N(CO)_{12}]$ (0.26 g, 0.37 mmol) and $[PPh_4][Rh(CO)_4]$ (0.20 g, 0.37 mmol) were dissolved in THF (20 mL) and refluxed for 4 h, monitoring the course of the reaction by IR. The solvent was dried in vacuum, and the residue was suspended in MeOH (20 mL). Solid $[PPh_4]Br$ (0.2 g) was added, and the mixture was stirred at room temperature to ensure complete precipitation. The microcrystalline powder was collected by filtration, washed with MeOH (2 × 5 mL), and dried. The crude product was extracted from the frit with minimum amount of THF (∼5 mL) and layered with 2-propanol, yielding 0.41 g (37%) of crystals suitable for X-ray analysis. Anal. Calcd for $C_{67}H_{48}Fe_5NO_{16}P_2Rh$: C, 51.07; H, 3.04; N, 0.89. Found: C, 51.12; H, 2.87; N, 0.99. The elemental analyses are in keeping with the presence of clathrated THF. IR (THF, ν(CO)): 2020 (w), 1954 (vs), 1890 (w), 1814 (m br) cm^{-1}.

Synthesis of $[PPh_4]_2[Fe_5IrN(CO)_{15}]$ (2a). $[NEt_4]_3[Fe_6N(CO)_{15}]$ (0.46 g, 0.40 mmol) was dissolved in CH_3CN (20 mL) at room temperature. Four portions of $[Ir(C_8H_{14})_2Cl]_2$ (0.16 g, 0.18 mmol each) were added every hour while stirring and monitoring by IR. When the reaction was completed, the mixture was filtered. The solvent was dried in vacuum, and the residue was treated as above. Yield: 0.45 g (72%) of crystals suitable for X-ray analysis.

The elemental analyses were unsatisfactory, and the product was further purified by dissolving the crystals in THF, filtering a black insoluble material, and layering with 2-propanol. Anal. Calcd for $C_{67}H_{48}Fe_5NO_{16}P_2Ir$: C, 48.6; H, 2.92; N, 0.85. Found: C, 48.3; H, 2.9; N, 0.87. The elemental analyses are in keeping with the presence of clathrated THF. IR (THF, ν(CO)): 2021 (w), 1953 (vs), 1890 (w), 1793 (m br) cm^{-1}.

Synthesis of $[NEt_4][Fe_4Rh_2N(CO)_{15}]$ (3d). $[PPh_4]_2[Fe_5RhN(CO)_{15}]$ (0.46 g, 0.31 mmol) and $RhCl_3 \cdot xH_2O$ (0.08 g, 0.37 mmol) were suspended in CH_3CN (20 mL) and refluxed while monitoring by IR. After 2 h, a second portion of $RhCl_3 \cdot xH_2O$ (0.06 g, 0.3 mmol) was added, and the mixture heated for 2 h more. The solvent was dried in vacuum, and the residue was dissolved in MeOH (25 mL). $[NEt_4]Br$ (1 g) and water (30 mL) were added while stirring, inducing precipitation of a microcrystalline solid, which was collected by filtration and washed with water (2 × 10 mL). To ensure complete ion exchange, the solid was again dissolved in MeOH and precipitated with $[NEt_4]Br$ and water; the final product was dried and crystallized from THF/cyclohexane. Yield: 0.20 g, 65%. Anal. Calcd for $C_{23}H_{20}Fe_4N_2O_{15}Rh_2$: C, 27.81; H, 2.03; N, 2.82. Found: C, 27.50; H, 2.32; N, 3.07.

The salt **3d** can be easily crystallized and purified; for this reason it was used for the most part of the chemical characterization. Unfortunately, its crystals are not suitable for X-ray analysis. Crystals of $[PPh_4][Fe_4Rh_2N(CO)_{15}]$ (**3c**) used for X-ray determination were obtained by the same procedure. Larger samples are usually impure, since this salt is extremely soluble in THF. IR (THF, ν(CO)): 2058 (vw), 2008 (vs), 2000 (s), 1977 (m), 1940 (w), 1861 (m) cm^{-1}. FABMS (negative ions): *m/z* 863 ($[Fe_4Rh_2N(CO)_{15}]^-$); 863 − 28*x* ($[Fe_4Rh_2N(CO)_{15-x}]^-$, $x = 1-8$).

X-ray Data Collection and Structure Determination. Crystal data and other experimental details are summarized in Table 8. The

(35) Martinengo, S.; Ciani, G.; Sironi, A. *J. Chem. Soc., Chem. Commun.* **1991**, 26.
(36) Shriver, D. F.; Dredzon, M. A. *The Manipulation of Air-Sensitive Compounds*, 2nd ed.; Wiley: New York, 1986.
(37) Fjare, D. E.; Gladfelter, W. L. *Inorg. Chem.* **1981**, *20*, 3533.
(38) Garlaschelli, L.; Della Pergola, R.; Martinengo, S. *Inorg. Synth.* **1991**, *28*, 211.
(39) Van Der Ent, A.; Onderdelinden, A. L. *Inorg. Synth.* **1991**, *28*, 91.
(40) Bianchini, C.; Laschi, F.; Masi, D.; Ottaviani, F. M.; Pastor, A.; Peruzzini, M.; Zanello, P.; Zanobini, F. *J. Am. Chem. Soc.* **1993**, *115*, 2723.

diffraction experiments were carried out on an Enraf-Nonius CAD-4 diffractometer at room temperature using Mo Kα radiation (λ = 0.710 73 Å) with a graphite crystal monochromator in the incident beam. The calculations were performed on a PDP 11/73 computer using the SDP structure determination package,[41] and the physical constants were tabulated therein. A periodic monitoring of three standard reflections revealed a crystal decay, on X-ray exposure, which was evaluated as about 23% for **1a**, 10% for **2a**, and 14% for **3c** (on intensities) at the end of data collection. The diffracted intensities were corrected for Lorentz, polarization, decay, and absorption effects (empirical correction).[42] Scattering factors and anomalous dispersion corrections were taken from ref 43. The structures were solved by direct methods (MULTAN)[44] and difference Fourier syntheses and refined by full-matrix least-squares, minimizing the function $\sum w(F_o - k|F_c|)^2$. Anisotropic thermal factors were refined for all the non-hydrogen atoms. In compounds **1a** and **2a**, the refinement of the occupancy factors of the metal sites revealed Rh−Fe and Ir−Fe disorder: thus, in **1a** the metal atom labeled Rh is 81% rhodium and 19% iron, with the remaining 19% rhodium equally distributed in the five metal sites labeled Fe(1)−Fe(5). A practically identical disorder is present in **2a**, where the metal atom labeled Ir is 82% iridium and 18% iron. In compound **3c**, the metal atoms of the **A** anion are ordered whereas in anion **B** the atom labeled Rh(2B) is 81% rhodium and 19% iron, with the remaining 19% rhodium equally distributed in the four metal sites labeled Fe(1B)−Fe(4B). In all cases, the hydrogen atoms of the cations and of the THF molecules were placed in their ideal positions (C−H = 0.97 Å, B = 1.20 times that of the carbon atom to which they are attached) and not refined. In compound **3c**, the refinement of the correct structure enantiomorph led to $R = 0.035$ and $R_w = 0.048$ whereas the refinement of the wrong one gave $R = 0.038$ and $R_w = 0.052$. The final Fourier maps showed maximum residuals of 0.83(7) e Å^{-3} at 0.98 Å from Fe(4) in compound **1a**, 2.80(10) e Å^{-3} at 1.78 Å from C(13) in **2a**, and 3.60(11) e Å^{-3} at 1.06 Å from Rh(1B) in **3c**. The atomic coordinates of the structure models are available from the authors.

Catalytic Runs. Hydroformylation experiments were carried out in a stainless steel autoclave (PARR 4841) equipped with a mechanical turbine stirrer, thermocouple, liquid sampling device, and glass liner to avoid direct contact of solutions with the stainless steel.[45]

In a typical experiment, the substrate (1.3 g) and the catalyst precursor (0.016 g) were dissolved in 15 mL of THF in a Schlenk tube under nitrogen, then introduced into the autoclave, which was then purged three times with a CO/H_2 mixture and brought under pressure.

The reaction times were measured when the apparatus reached the selected temperature, and the liquid phase was periodically spilled and analyzed by IR and GLC. The reaction was then quenched by cooling the autoclave in an ice bath and depressurizing. The final mixtures were analyzed by gas chromatography on a Hewlett-Packard 4890/II equipped with 3396/II HP integrator using a Poraplot Q column (25 m × 0,53 mm). The products were identified using GC/MS HP 5971A.

Acknowledgment. A.C. gratefully acknowledges the financial support by CNR of Italy. P.Z. acknowledges the financial support by EEC (HCM programme; contract No. CHRX CT93 0277).

Supporting Information Available: IR spectrum of $[PPh_4]_2[Fe_5Ir(CO)_{15}]$ in THF, and tables of atomic coordinates, anisotropic thermal parameters (Us) for the non-hydrogen atoms, and crystallographic data for compounds **1a**, **2a** and **3c** (19 pages). Ordering information is given on any current masthead page.

IC961451G

(41) Frenz, B. A. et al. *SDP Plus*, Version 1.0; Enraf-Nonius: Delft, The Netherlands, 1980.
(42) North, A. C. T.; Phillips, D. C.; Mathews, F. S. *Acta Crystallogr., Sect. A* **1968**, *24*, 351.
(43) *International Tables for X-ray Crystallography*; Kynoch Press: Birmingham, England, 1974; Vol.4,
(44) Main, P.; Fiske, S. J.; Hill, E.; Lessinger, L.; Germain, G.; Declercq, J. P.; Wolfson, M. M. *MULTAN 80, a system of computer programs for the automatic solution of crystal structures from X-ray diffraction data*; Universities of York (England) and Louvain (Belgium), 1980.
(45) Della Pergola, R.; Garlaschelli, L.; Martinengo, S.; Repossi, A. *J. Mol. Catal. A* **1997**, *115*, 265.